Transverse and Polarization Mode Selection in VCSELs

Josep Mulet*[a], Claudio R. Mirasso[b], Salvador Balle[a], and Maxi San Miguel[a]

[a] Instituto Mediterraneo de Estudios Avanzados, IMEDEA, (CSIC-UIB)
E-07071 Palma de Mallorca, Spain.
[b]Department de Física, Universitat de les Illes Balears, E-07071 Palma de Mallorca, Spain.

ABSTRACT

We develop a mesoscopic model of semiconductor dynamics for vertical-cavity surface-emitting lasers which allows us to describe polarization and transverse mode dynamics simultaneously. Within this model, we study the selection processes and the turn-on delay for the switch-on of different transverse modes in gain-guided VCSELs. We consider different active-region diameters, excitation conditions and current shapes. Following the application of the current pulse, transverse modes become excited in a quite definite sequence. After the turn-on, the VCSEL initially switches-on in the fundamental transverse mode, but higher-order transverse modes become excited later. In general, the results obtained are in qualitative agreement with experiments reported recently. Finally, we discuss the current shape dependence on the transverse mode selection at threshold.

Keywords: VCSEL, Transverse Modes, Laser Switch-on, Polarization Effects

1. INTRODUCTION

Vertical-cavity surface-emitting lasers (VCSELs) are promising novel devices suitable in many optical applications. VCSELs are specially interesting due to their single-longitudinal emission, easy integration in 2D arrays, and narrow circular output beams. Aside from these advantages, many fundamental questions have been devoted the attention of many research groups: light-polarization instabilities, enhanced quantum fluctuations, and excitation of higher-order transverse modes among others. In addition, the necessity of high power lasers modulated at high frequencies enhances the multimode[1] behavior of the VCSEL modifying the spectral, spatial and noise characteristics. In particular, the development of strategies to avoid multimode oscillation in large aperture devices is interesting for applications. On the other hand, multimode operation of the VCSEL is useful in multimode fiber links in order to reduce the modal noise.[2] All these facts motivates the study, characterization and control of transverse mode dynamics.

It is known that transverse modes properties of VCSELs are determined by a complex interplay of gain profile, carrier-induced refractive index, diffraction, temperature distribution and eventually by a built-in index waveguiding. Furthermore, it is quite usual that many of this contributions become relevant at the same order being impossible to determine the dominant mechanism. The gain profile is linked to the spatial distribution of the carrier density in the quantum well (QW) which is modified by spatial hole burning, carrier diffusion and shape of the electrical contacts. Also the active material provides a carrier-induced refractive index that arises from the real part of the susceptibility function. The carrier-induced refractive index of a QW is carrier-antiguiding, i.e. the refractive index decreases when the carrier density increases. The lateral confinement of the optical field occurs via a combination of gain guiding and index antiguiding effects.[3] Therefore, analytical expressions for the QW susceptibility[4] have supposed a considerable improvement of previous works describing the active material in terms of a Lorentzian response function.[5] The inhomogeneous injection of current preferably close to the cavity axis generates, via Joule heating, a temperature distribution. Through the temperature dependence of the background refractive index a thermal lensing (TL) is generated providing an optical waveguide that tends to laterally confine the optical mode. Thermal lensing is an important mechanism to determine the transverse mode properties of gain-guided VCSELs with no built-in refractive index contribution.[6,7] In general, we have found that the thermal lensing modifies significantly these results[7] being responsible, among other things, of the tendency towards a multimode emission and the typical frequency splitting between transverse modes.

In this paper, we take advantage of the mesoscopic model[7–9] of semiconductor dynamics of VCSELs that describes simultaneously polarization and transverse effects. We study the transient response of gain-guided VCSEL subjected

*Correspondence: Email: mulet@imedea.uib.es; WWW: http://www.imedea.uib.es/PhysDept; Telephone: +34 971 172536; Fax: +34 971 173426

Physics and Simulation of Optoelectronic Devices IX, Yasuhiko Arakawa, Peter Blood, Marek Osinski, Editors, Proceedings of SPIE Vol. 4283 (2001) © 2001 SPIE · 0277-786X/01/$15.00

to short electrical pulses. We analyze the turn-on delay, i.e. switch-on time difference between a higher-order transverse mode with respect to the fundamental one. We present a systematic dependence of the turn-on delay as function of the amplitude of the current pulse for two different active region diameter VCSELs. The motivation is mainly addressed to recent experimental investigations of the transient response of gain-guided VCSELs excited by fast electrical pulses.[10–12]

2. THE MODEL

We consider that the VCSEL cavity only supports one longitudinal mode and that the field is almost polarized orthogonal to the cavity axis. Under this situation, the circularly-polarized components of the optical field inside the cavity can be written as follows

$$\mathcal{E}_{\pm}(\vec{r},t) = \left(e^{iqz} + \frac{e^{-iqz}}{r_1}\right) A_{\pm}(\vec{r}_{\perp};t)e^{-i\Omega t}. \tag{1}$$

$A_{\pm}(\vec{r}_{\perp};t)$ represent the transverse dependence of the slowly-varying optical fields in both circular polarization components. The propagation constant q of the longitudinal mode is determined by the boundary conditions at the top and bottom Bragg mirrors. Ω stands for the optical frequency of the longitudinal mode of the cold VCSEL cavity. We also need equations for the carrier densities $N_{\pm}$ associated with electron population of different spin orientation that tend to be equalized by spin flip processes at rate γ_J. The emission of left(right) polarized photons is linked to recombination transitions of $N_+(N_-)$ electrons. The optical fields $A_{\pm}(\vec{r}_{\perp};t)$ and carrier densities normalized to the transparency value, $D_{\pm}(\vec{r}_{\perp};t) = N_{\pm}(\vec{r}_{\perp};t)/N_t$, evolve according to[7]

$$\begin{aligned}\partial_t A_{\pm} &= -\kappa A_{\pm} + i\mathcal{L}A_{\pm} + i\frac{a\Gamma}{2}\chi_{\pm}\left(\Omega + i\tfrac{\partial_t A_{\pm}}{A_{\pm}}, D_+, D_-\right)A_{\pm} \\ &\quad -(\gamma_a + i\gamma_p)A_{\mp} + \sqrt{\beta D_{\pm}}\,\xi_{\pm}(x,y;t),\end{aligned} \tag{2}$$

$$\begin{aligned}\partial_t D_{\pm} &= \mu(t)C(r)\gamma_e/2 - \gamma_e D_{\pm} - (BN_t)D_{\pm}^2 \mp \gamma_J(D_+ - D_-) \\ &\quad +\mathcal{D}\nabla_{\perp}^2 D_{\pm} + a\,\mathrm{Im}\chi_{\pm}\left(\Omega + i\tfrac{\partial_t A_{\pm}}{A_{\pm}}, D_+, D_-\right)|A_{\pm}|^2,\end{aligned} \tag{3}$$

where

$$\chi_{\pm}(\Omega+\omega, D_+, D_-) = -\chi_0\left[\ln\left(1 - \frac{2D_{\pm}}{u+i}\right) + \ln\left(1 - \frac{D_+ + D_-}{u+i}\right) - \ln\left(1 - \frac{b}{u+i}\right)\right], \tag{4}$$

is an analytical approximation to the susceptibility of a QW[4] medium in the presence of a circularly polarized field, $A_{\pm}$. The frequency dependence of the susceptibility is included through $u \equiv (\Omega+\omega-\omega_g)/\gamma_{\perp} + \sigma(D_- + D_+)^{1/3} \equiv \Delta + \sigma(D_- + D_+)^{1/3} + \omega/\gamma$. Δ is the normalized frequency detuning of the VCSEL's longitudinal mode with respect to the bandgap, ω is the difference between the actual VCSEL emission frequency and the longitudinal mode frequency, and $\sigma(D_- + D_+)^{1/3}$ phenomenologically describes bandgap renormalization due to Coulomb interaction between electrons and holes. The gain coefficient a in Eq. 2 is given by $a = \Omega/(n_e n_g)$ where n_e and n_g are the background and group refractive index respectively. The optical frequency Ω is corrected by the "instantaneous frequencies", $i\frac{\partial_t A_{\pm}}{A_{\pm}}$, that appear in $\chi_{\pm}(\Omega + i\frac{\partial_t A_{\pm}}{A_{\pm}}, D_+, D_-)$; such a term[8] accounts for the changes in the susceptibility due to nonlinearities and variations experienced by different transverse modes due to the different modal frequencies.

We consider that the optical field inside the VCSEL cavity is polarized in an arbitrary direction orthogonal to the cavity axis. However, cavity anisotropies (birefringence and dichroism) break the circular symmetry and select two preferred orthogonal orientations $\hat{x}$ and $\hat{y}$ related to the crystallographic axis. Birefingence provides a frequency splitting between the $\mathrm{LP}_{\hat{x}}$ and $\mathrm{LP}_{\hat{y}}$ linearly polarized states and dichroism reduces the effective losses of $\mathrm{LP}_{\hat{y}}$ with respect $\mathrm{LP}_{\hat{x}}$ (for $\gamma_a > 0$). We use the circular representation of the optical fields $A_{\pm}$ since the QW-interaction is expressed in this basis, nevertheless the relationship between the two basis is given by $A_{\pm} = (A_x \pm iA_y)/\sqrt{2}$. The inhomogeneities in background index distribution are included by means of the waveguide operator

$$\mathcal{L}A_{\pm} = \frac{c^2}{2\Omega n_e n_g}\left[\nabla_{\perp}^2 + \left(\frac{\Omega}{c}\right)^2 2n_e\Delta n(\vec{r}_{\perp};\Omega)\right]A_{\pm}, \tag{5}$$

where n_e is the homogeneous background index of the passive material filling the cavity, and $\Delta n(\vec{r}_\perp;\Omega) << n_e$ is the excess refractive index distribution. As will be discussed latter, this lateral variation of the refractive index arises from the thermal lensing effect.

The radial variation of the current shape is defined by the function $C(r)$, while $\mu(t)$ allows us to apply current pulses in such a way that the total injected current reads

$$I(t) = q\gamma_e N_t W \mu(t) 2\pi \int_0^\infty r dr C(r), \tag{6}$$

being q the electronic charge and W the width of the QW. The spatial extended spontaneous emission, with rate β, is modeled using Gaussian random numbers with zero mean and correlation $\langle \xi_\pm^*(x_i, y_j, t)\xi_\pm(x_{i'}, y_{j'}, t')\rangle = 2\delta_{i,i'}\delta_{j,j'}\delta(t-t')$. We integrate the spatio-temporal dynamics using a spectral method that treats the linear terms of the Eq. (2) exactly and the non-linear terms at first order in Δt. The integration region is large enough, 80×80 μm^2 on a grid of 128×128 points, to avoid spurious re-injection of the variables at the boundaries. The meaning and values of the different parameters involved in equations (2)-(4) are listed in Table 1.

Symbol	Meaning	Value
$a\chi_0$	effective gain constant	$1.3 \cdot 10^4$ns^{-1}
Γ	confinement factor	0.045
γ	material polarization decay	20 ps^{-1}
n_e	background refractive index	3.3
n_g	group refractive index	3.5
λ	free-space wavelength	0.85 μm
σ	bandgap shrinkage	0.2
b	unpumped contribution to χ	10^4
κ	cavity loses	300 ns^{-1}
γ_a	linear dichroism	0.5 ns^{-1}
γ_p	linear birefringence	30 ns^{-1}
γ_e	non-radiative recombination rate	1.0 ns^{-1}
BN_t	bimolecular recombination rate	0.1 ns^{-1}
γ_J	spin flip rate	50 ns^{-1}
$\mathcal{D}$	bimolecular diffusion	0.3 μm$^2/ns$
β	spontaneous emission rate	10^{-5} ns^{-1}

Table 1. Symbols, meaning and values of some parameters.

2.1. A simple thermal model

A uniform increment of the substrate temperature T_b produces a redshift of the longitudinal mode resonance with respect to the nominal transition frequency. The final result appears as an enhancement of the detuning when the substrate temperature is increased; $\Delta(T_b) = \Delta_0 + v\ (T_b - T_0)$ with $v \sim 3\times10^{-2}$ K^{-1}. Nevertheless, the temperature distribution in a VCSEL is not uniform because the Joule heating is predominantly produced close to the cavity axis. When a non-uniform distribution of the temperature $\Delta T(\vec{r}_\perp)$ is superposed onto the substrate temperature, it translates to refractive index providing the cavity modal profiles, modal frequencies and a redshift as well.

For sake of simplicity, we approximate the thermal lensing by a radial distribution with parabolic shape. Therefore, the refractive index distribution can be written as $\Delta n(r) = \Delta n_{tl}\left[1-(2r/\phi_g)^2\right]$ if $r \le \phi_g/2$ and $\Delta n(r) = 0$ elsewhere. In a first approximation we assume that the specific susceptibility parameters χ_0, b, and σ are temperature independent for the whole range of temperatures under study.

The cavity modes in the weak-guidance approximation are determined by the eigenvalue equation

$$\left[\nabla_{\perp}^2 + \left(\frac{\Omega}{c}\right)^2 2n_e\Delta n(r)\right]\Phi_{ml} = W_{ml}\Phi_{ml}. \tag{7}$$

The modes LP_{ml} of Eq. 7 can be expressed as a series expansion of $R \equiv 2r/\phi_g < 1$ and read[13]

$$\Phi_{ml}(R,\theta) = \begin{cases} \frac{\sum_{n=0}^{\infty} a_n R^{n+l}}{\sum_{n=0}^{\infty} a_n} & \text{if} \quad \mathrm{R} < 1 \\ \frac{K_l(W_{ml}R)}{K_l(W_{ml})} & \text{if} \quad \mathrm{R} \geq 1 \end{cases} \times \begin{cases} \cos(l\theta) & \text{even mode} \\ \sin(l\theta) & \text{odd mode} \end{cases} \tag{8}$$

where K_l is a second kind Bessel function of order l, being $l = 0, 1, \cdots$ the angular number. The coefficients a_n in the wavefunction expansion are a_0 arbitrary, $a_{2n-1} = 0$ and

$$\begin{aligned} a_2 &= -\tfrac{(V^2 - W_{ml}^2)a_0}{4(l+1)} \\ a_{2n} &= \tfrac{1}{4n(n+l)}\left(V^2 a_{2n-4} - (V^2 - W_{ml}^2)a_{2n-2}\right) \quad \text{if} \quad \mathrm{n} \geq 2. \end{aligned} \tag{9}$$

The waveguide parameter is $V = (2\pi/\lambda)\ (\phi_g/2)\sqrt{2n_e\Delta n_{tl}}$. The propagation constants W_{ml} of the guided modes are obtained imposing continuity of $\Phi_{ml}(R,\theta)$ at $R = 1$. For each value of the angular number l, one has to solve a transcendental equation for W_{ml} that reads

$$W_{ml}\frac{K_{l+1}(W_{ml})}{K_l(W_{ml})} = -\frac{\sum_{n=0}^{\infty} n a_n}{\sum_{n=0}^{\infty} a_n}. \tag{10}$$

For any guided mode we have $0 \leq W_{ml} \leq V$ being W_{ml} maximum for the fundamental mode LP_{10}. The modal frequencies referred to Ω are[7] $\omega_{ml} = -\frac{2c^2}{\Omega n_e n_g}\left(\frac{W_{ml}}{\phi_g}\right)^2$. Since the frequency of the fundamental mode is $\omega_{10} < 0$, a redshift appears being much larger when the thermal lensing Δn_{tl} (or equivalently V) is enhanced.

In conclusion, for a given longitudinal mode detuning, $\Delta(T_b)$, different amounts of thermal lensing, Δn_{tl}, produce additional redshift related to the frequency position of the fundamental mode ω_{10}. Noteworthy, such a redshift will be negligible only for a device with an effective radial dissipation of the heat.

3. RESULTS

In this section we present the numerical results[14] obtained for the transient response of gain-guided VCSELs. The excitation consists in a current pulse of 1 ns of duration and 50 ps of rise and fall times. The bias current is chosen below threshold ($\mu_b = 0.85\ \mu_{th}$) and the 'on' current runs from threshold to well above threshold ($\mu_{on} \sim 1 - 9\ \mu_{th}$). Since the pulse duration is much shorter than the thermal time ($\tau_t \sim 1\mu$s), we can assume that the heat dissipated by the bias current provides the mean value of the thermal lensing. We have taken $\Delta n_{tl} = 4 \times 10^{-3}$ that, for GaAs based materials, roughly corresponds to a temperature increment of $\Delta T \sim 10$ K between the cavity axis and the substrate. The structure of this section is the following: In Sec. 3.1 we describe the results obtained for a small active region VCSEL (VCSEL A). In Sec. 3.2 we present the results for a larger device (VCSEL B). Finally, in Sec. 3.3 we discuss the effect of the current shape on the transverse mode selection close to threshold.

3.1. Results for the VCSEL A

We consider the VCSEL A with active region diameter $\phi_c = 12.5\ \mu$m and thermal lensing diameter $\phi_g = 12.5\ \mu$m. The lateral variation of the injected current has a super-Gaussian shape of the form $C(r) = e^{-(2r/\phi_c)^6}$. The total injected current is determined from Eq. 6, $I(t) = \frac{\pi}{12}\Gamma[1/3]q\gamma_e N_t W\phi_c^2\mu(t)$. The threshold current can be analytically determined[7] as soon as the operating detuning is chosen (in our case it corresponds to $\Delta = 0.5$). It is important to point out that this detuning only accounts for the frequency difference between the longitudinal mode and the transition frequencies and therefore does not contain the additional frequency shift induced by the thermal lensing and by the carrier-induced refractive index. For this operating conditions the threshold current in dimensionless units is found to be $\mu_{th} = 2.6$. The numerical simulations start from initial conditions that correspond to the "off" state biased at $\mu_b = 0.85\mu_{th}$.

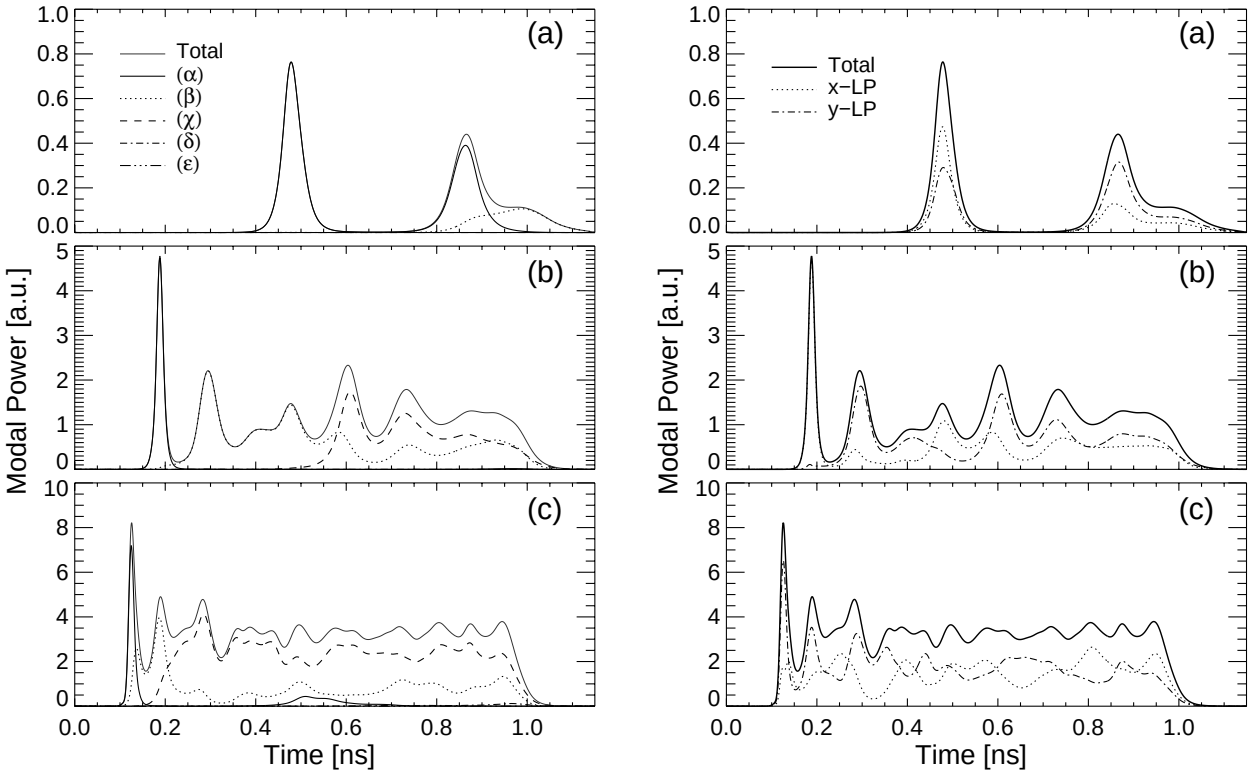

Figure 1. VCSEL A: (Left) Time evolution of the power of the transverse modes for three different values of the current pulse (a) $\mu_{on} = 1.5\mu_{th}$, (b) $\mu_{on} = 4\mu_{th}$ and (c) $\mu_{on} = 9\mu_{th}$. (Right) Time evolution of the total power and power in each orthogonal polarization $\mathrm{LP}_{\hat{x},\hat{y}}$ for the same situations than before.

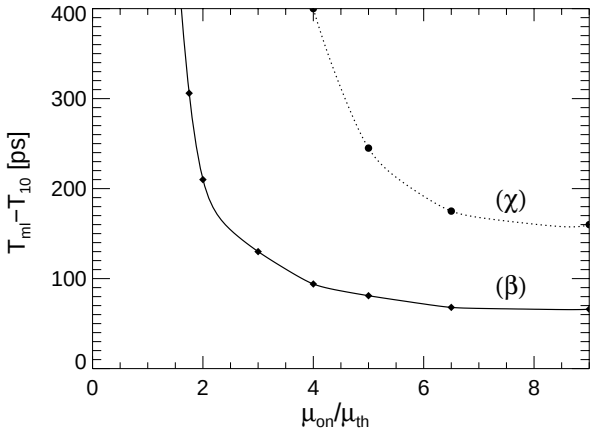

Figure 2. Turn-on delay of the transverse modes of the VCSEL A.

In Fig. 1 we show the optical response of the VCSEL when a current pulse is switched-on at $t = 0$. We numerically integrate the partial differential Eqns. (2)-(3) and we compute, by a filtering technique, the time evolution of each transverse mode separately [see Appendix A]. The left panels in Fig. 1 describe the non-polarization resolved evolution of the optical power of each transverse mode for three values of the "on" current of the pulse: (a) $\mu_{on} = 1.5\mu_{th}$, (b) $\mu_{on} = 4\mu_{th}$, and (c) $\mu_{on} = 9\mu_{th}$. The transverse modes are labeled as follows: (α) is the fundamental LP_{10} mode,

(β) is the first-order excited LP_{11} mode, (χ) is a combination of transverse modes $LP_{12} + LP_{20}$, etc. The typical frequency separation between transverse modes is ~ 100 GHz. In general, the states (δ) and (ϵ) are also combination of several higher-order transverse modes. The modes with the same value of $(2m + l - 1)$ appear nearly degenerate in the optical spectrum[15] and we are not able to obtain their separate evolution due to resolution limitations in the filtering process. In the three cases, we observe that the laser switches-on in the Gaussian fundamental transverse mode (LP_{10}). The first peak in the optical power burns carriers at the center of the carrier distribution. The laser starts to develop the first relaxation oscillation whose frequency increases for higher 'on' currents. In (a) the Gaussian mode is also excited during the second relaxation oscillation but this oscillation accompanies the excitation of the first-order transverse mode. There is a time interval where both transverse modes compete for the available gain but as soon the current is turned-off (at $t = 1$ ns) we observe that the laser switches-off in the first-order transverse mode. Moreover, the final spatial distribution of the carrier densities displays a hole in the center region due to spatial-hole burning. In (b) and (c), immediately after the fist optical peak, the Gaussian mode switches-off and the first order transverse mode (LP_{11}) starts to lase. The LP_{11} mode starts to oscillate at its relaxation frequency burning carriers in a outer ring of the center region. After some time, the mode LP_{11} has burned carriers causing a hole deep enough to favor the excitation of higher-order transverse modes. We observe the state (χ) appearing at $t = 0.55$ ns and emitting simultaneously with the state (β). Both modes approach with the same amount of power to the "off" state when the current is turned-off. A similar behavior can be observed in (c) but within smaller time scales. Looking with more detail at the first optical peak, we can see a small time interval when the fundamental and first order transverse mode compete. Another observation is that the coexistence of (β) and (χ), during a time interval (0.4-0.6 ns), is accompanied by the sudden appearance of the fundamental mode. This effect is due to the fact that the dominant mode (χ) burns carriers far away from the center of the carrier distribution providing the required gain for the fundamental mode to lase. The right panels of Fig. 1 show the evolution of the total optical power emitted and the optical power in both orthogonal polarizations $LP_{\hat{x}}$ and $LP_{\hat{y}}$. We can see that both polarization are active during all the transient having a similar evolution for the three cases.

One interesting quantity that deserves to be considered is the turn-on delay of the high-order transverse modes. Let T_{ml} be the switch-on time of the transverse mode LP_{ml}. The turn-on delay of such a mode is defined as the switch-on time referred to the switch-on time of the fundamental mode, i.e. $\Delta T_{ml} = T_{ml} - T_{10}$. It is also interesting to investigate the variations of ΔT_{ml} on the applied current pulse. In Fig. 2 we plot the turn-on delay of the transverse modes (β) and (χ) as function of the "on" current, μ_{on}. As expected the turn-on delay for all the modes rapidly increases when approaching to threshold, displaying an asymptotic behavior above $\mu_{on} > 1$. Another peculiar property is that after the application of the current pulse, the transverse modes appear in a quite definite sequence. For this reason, we always find that the turn-on delay increases when increasing the order of the transverse mode for any value of the current pulse. Simple analytical expressions for the turn-on delay were already reported[11] in terms of an independent mode theory. However, we note that such kind of modeling losses realism when calculating the turn-on delay of successive excited transverse modes. This is because such a model does not take into account the spatial hole burning, an effect that we find to be the determinant mechanism to explain the delay onset of the switch-on of the transverse modes.

3.2. Results for the VCSEL B

The VCSEL B has a larger active region diameter, $\phi_c = 22$ μm, and thermal lensing diameter is $\phi_g = 30$ μm. We take ϕ_g larger than ϕ_c to mimic the heat diffusion across the cavity axis. The thermal lensing strength has been also set to $\Delta n_{tl} = 4 \times 10^{-3}$ yielding typical frequency separation between transverse modes of 45 GHz. Large aperture devices have more gain available at the periphery. Since this fact favors the threshold condition of higher-order transverse modes, we expect higher multitransverse mode behavior specially under pulsed operation. In Fig. 3 we plot the time evolution of the different transverse modes for identical excitation conditions than Fig. 2. Comparing with Fig. 2, we can see that in general a larger number of modes are excited by the pulse. As soon as the transverse modes are excited, they prefer to compete all together instead of transferring the power from one mode to the next higher-order mode. For this reason we see in Fig. 3(c) that the fundamental transverse mode maintains a non-negligible intensity value during a large part of the time. In addition, the turn-on delays are considerably reduced in all the situations [See Fig. 4]. Furthermore, it has been experimentally observed[10,11] that decreasing the bias current the turn-on delay of the transverse modes increases. For this VCSEL B and only for currents higher than $\mu_{on} = 7\mu_{th}$ we observe that the first-order transverse mode starts to lase first with a very small turn-on delay compared with the fundamental one. The same kind of behavior was found in the experiment of a 22 μm gain-guided AlGaAs-GaAs multiple-quantum

well VCSEL being this behavior attributed to a slightly annular shape of the current distribution.[11] We will discuss in Sec. 3.3 the effect of a ring current shape in the transverse mode selection close to threshold.

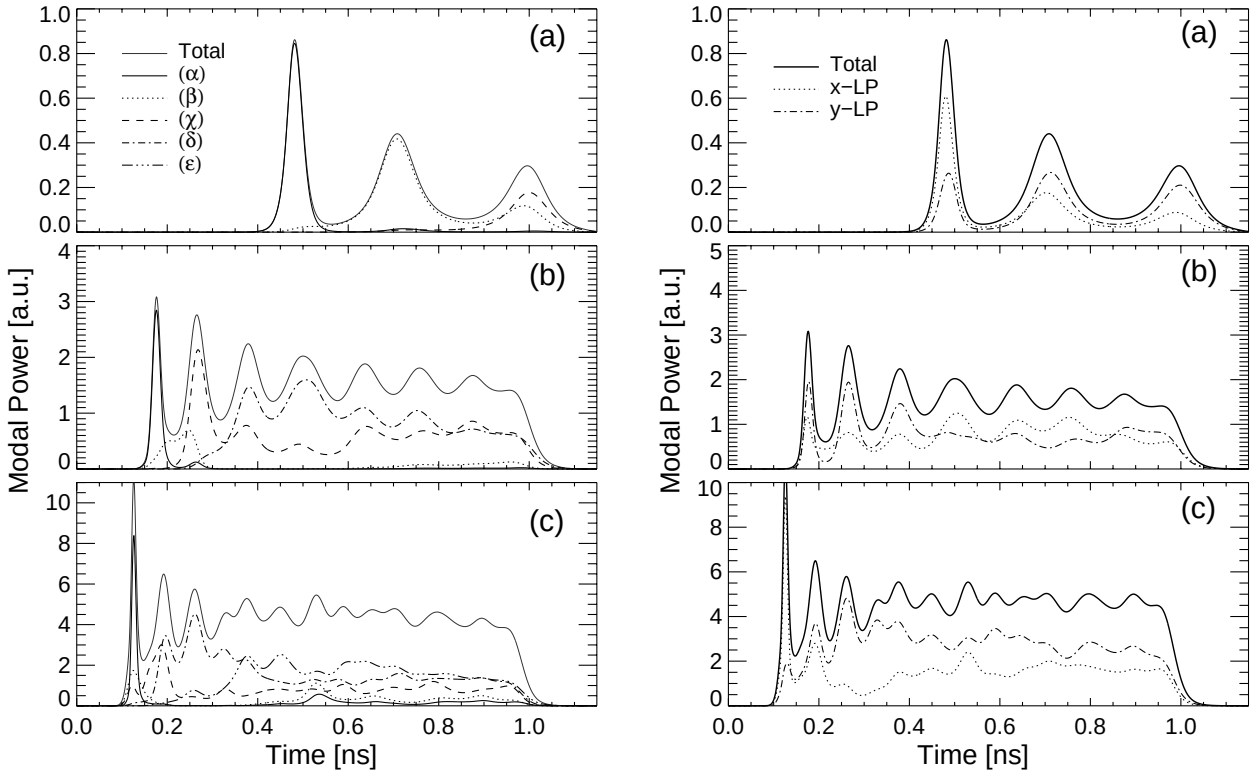

Figure 3. VCSEL B: (Left) Time evolution of the power of the transverse modes for (a) $\mu_{on} = 1.5\mu_{th}$, (b) $\mu_{on} = 4\mu_{th}$ and (c) $\mu_{on} = 9\mu_{th}$. (Right) Time evolution of the total power and power in orthogonal polarization.

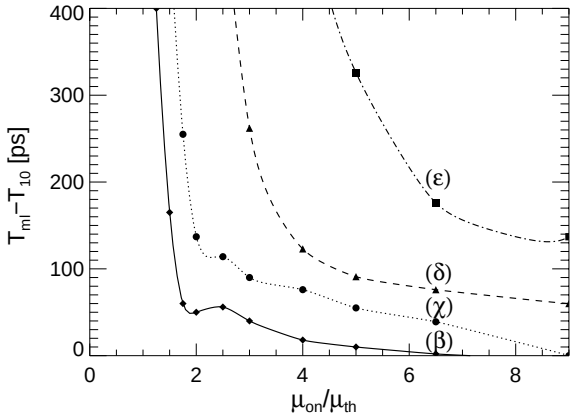

Figure 4. Turn-on delay of the transverse modes of the VCSEL B.

In general, we have found qualitative good agreement for the dependence of the turn-on delay versus the current pulse between the numerical and experimental results. Notwithstanding, it is important to point out that this agreement is only possible if thermal lensing is considered. Otherwise, a lesser number of modes with longer turn-on delays would be observed.[7]

3.3. Current shape dependence

Within our model, we are able to analytically determine the threshold of the different transverse modes for any functional form of the current shape, $C(r)$. In this section we study how the current shape modifies the selection of transverse modes close to threshold. The analytical results are accompanied by numerical simulations to check the validity of the calculations. We consider a device with the same intrinsic parameters than the VCSEL A discussed in Sec. 3.1 but allowing to chose different current shapes. The numerical simulations start from initial conditions corresponding to the steady state slightly below threshold. At $t = 0$ a current step is applied from $0.9\mu_{th}$ to $1.1\mu_{th}$ and the laser is forced to operate detuned by $\Delta = 0.1$ from the transition frequency.

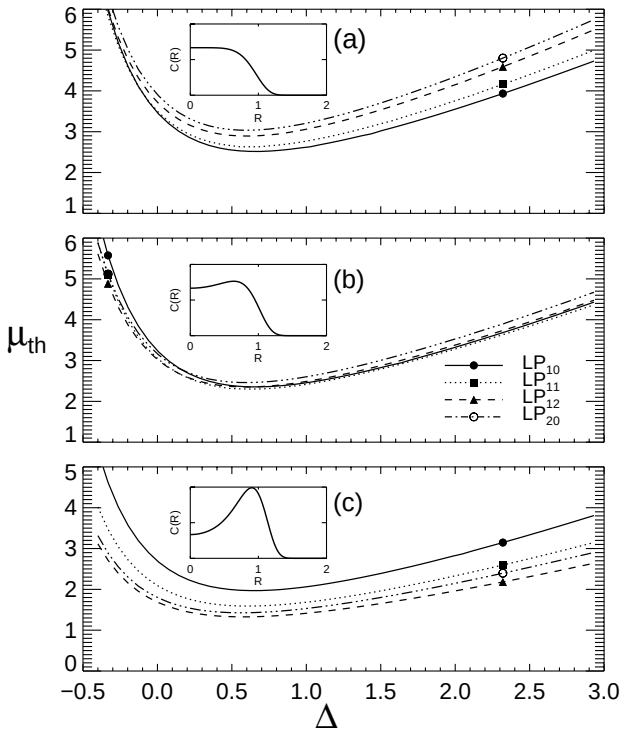

Figure 5. Threshold curves of some transverse modes for different current shapes: (a) super-Gaussian, (b) slightly ring, (c) ring shape. The 12 μm active-region VCSEL operates detuned by Δ=0.1.

We compute the threshold current of the different LP_{ml} modes that satisfies[7] the following set of equations

$$-i\omega^{nl} = -\kappa + i\frac{a\Gamma}{2}\frac{\int\int \chi\left(\Omega + \omega_{ml} + \omega^{nl}, D_{th}(r)\right)|\Phi_{ml}|^2 \; d^2\vec{r}}{\int\int |\Phi_{ml}|^2 \; d^2\vec{r}} \tag{11}$$

$$0 = \mu_{th}C(r)\gamma_e/2 - \gamma_e D_{th} - (BN_t)D_{th}^2 + \mathcal{D}\nabla_\perp^2 D_{th} \; . \tag{12}$$

From these equations we can obtain the dimensionless threshold current μ_{th} and the non-linear frequency shift ω^{nl} of the transverse mode LP_{ml} under consideration. In Fig. 5, we plot the threshold current of the fundamental transverse mode (LP_{10}) and some higher-order transverse modes. In what follows we change the shape of the radial variation of the current, going from a super-Gaussian shape $C(r) = e^{-\varrho^6}$ in (a), through a slightly annular shape $C(r) = e^{-\varrho^6} \; e^{\varrho^2/2}$ in (b) and ending with a sharp ring shape $C(r) = e^{-\varrho^6} \; e^{2\varrho^2}$ in (c) being $\varrho = 2r/\phi_c$. In Fig. 5(a) the Gaussian mode has the lowest threshold (or the highest modal gain) for all the range of detunings depicted. We point out that different values of Δ are linked to different values of the substrate temperature but with the same thermal lensing strength Δn_{tl}. The horizontal axis corresponds to a substrate temperature variation of $\sim$ 100 K. The threshold current of the successive high-order transverse modes increases indicating a worse overlap between the modal profile and the carrier distribution. For negative detunings and due to the strong variation of the red-side

gain curve on carrier density, the lack of overlapping is compensated by the material gain differences experimented by different transverse modes. The numerical simulation in Fig. 6(a) indicates that the laser action starts from a circularly symmetric spontaneous emission near field. The laser switches-on undergoing relaxation oscillations but remains always in the Gaussian fundamental transverse mode. For the intermediate current shape depicted in Fig. 5(b), the slightly annular shape of the current reduces the threshold of the higher-order transverse modes compared with the fundamental one. This situation is such that several modes have similar threshold currents and a competition between them is expected. However, for $\Delta = 0.1$ the first-order transverse mode LP_{11} has the lowest threshold current. The numerical simulation in Fig. 6(b) indicates that the laser starts to emit spontaneous emission in the LP_{11} mode. However, the Gaussian mode appears as soon the optical power starts to display the first peak. Following the response to the current step, we see that the Gaussian mode disappear and the LP_{11} mode starts to lase again. This very interesting behavior is due to a small redistribution of the optical gain across the active region during the transient, that is able to favor the appearance of the Gaussian mode. The most surprising effect of a sharp ring current shape can be seen in Fig. 5(c). In this case, the fundamental transverse mode is unfavored due to the poor overlapping of the Gaussian mode with the ring-shaped carrier distribution. On the contrary, the ring-shaped carrier distribution enhances the modal gain of higher-order transverse modes, providing a lowest threshold for these modes. Furthermore, we can see that there is no intersection between the threshold curves in 5(c) indicating that the modal gain differences are dominated by geometrical considerations instead of different material gains. The analytical prediction is that the four-lobed LP_{12} mode has the lowest threshold curve being very much lower than the Gaussian mode. This is corroborated by the numerical simulation shown in Fig. 6(c) where the four-lobed mode arises from a non-circularly symmetric spontaneous emission near field. The LP_{12} mode can be clearly seen at the position of the first optical peak ($t \sim 1$ ns) and at later times but with the lobes rotated. This rotation can be regarded as a combination of even and odd LP_{12} modes whose weight coefficients depend on time.

Summarizing, we have introduced an analytical method that allows us to determine the threshold curves of different transverse modes. Despite the simplicity of this method, that in principle does not contain any information about the dynamics during the transient, it has been found to be a good indicator that determines the transverse mode selected close to threshold.

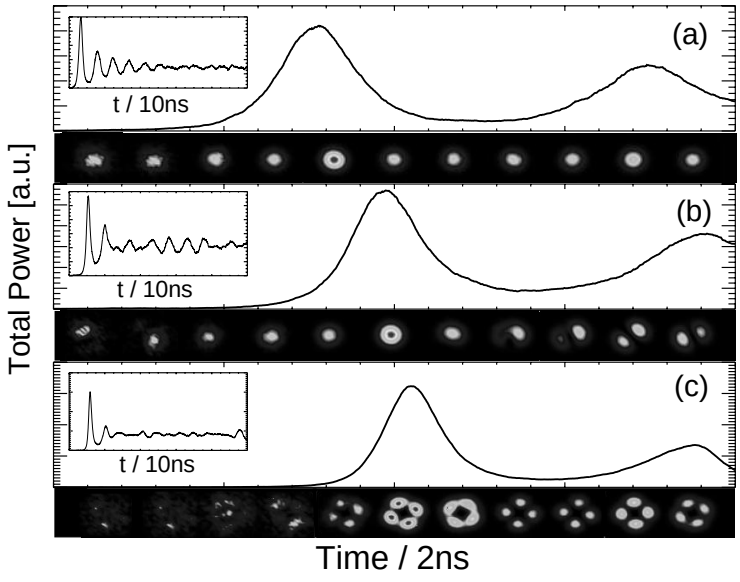

Figure 6. Numerical evolution of the non-polarization resolved near fields for the same conditions of Fig. 5.

4. CONCLUSIONS

The evolution of the optical power of different transverse modes of VCSELs subjected to short current pulses has been studied within a mesoscopic model. Our spatio-temporal dependent model describes temperature effects through

the thermal lensing and a temperature-dependent detuning. We have considered different pulse amplitudes in two VCSELs of different active region diameters. We have found a delay onset for the appearance of the transverse modes that compares quite well with the experiments. The turn-on delay and its dependence on the current pulse is also in agreement with the experimental results only when taking into account the thermal lensing effect. The existence of the turn-on delay has been explained in terms of spatial hole burning. The transverse mode selection close to threshold, for different current shapes, has been explored within analytical and numerical approaches. We have found that the threshold curves of the transverse modes are good indicators to determine the mode that will be selected close to threshold.

Generally speaking, the model presented in this paper provides an accurate description of VCSEL dynamics within a relatively simple mesoscopic framework, allowing to analyze polarization and transverse mode dynamics and selection in an unified way without a priori restrictions on the modal profiles and frequencies.

ACKNOWLEDGMENTS

This work has been funded by the European Commission through the VISTA HP-TMR network. Authors also acknowledge the Comisión Interministerial de Ciencia y Tecnología under project TIC98-0418-C05-02.

APPENDIX A. FILTERING TECHNIQUE

The optical spectrum of a discrete spatio-temporal field $\left\{E^n_{i,j}\right\}$ for $i = 1, \cdots, N_x$; $j = 1, \cdots, N_y$ and $n = 1, \cdots, N$ with $N = 2^k$ points can be computed from

$$S_E(\omega) \equiv \left| \frac{1}{NxNy} \sum_{i,j} \left(\hat{E}_{i,j}(\omega_n) \right) \right|^2 , \tag{A1}$$

being $\hat{E}_{i,j}(\omega_n) = \mathcal{F}E^n_{i,j}$ the direct fast Fourier transform of a discrete time series. From the peaks of the function $S_E(\omega)$ we determine the frequency positions, ω_k, of the different transverse modes. Now, we apply a second order filter $F(\omega;\omega_k)$ around the desired mode frequency and we isolate its time evolution $P_k(t_n)$ from

$$P_k(t_n) = \left| \frac{1}{NxNy} \sum_{i,j} \mathcal{F}^{-1} \left(\hat{E}_{i,j}(\omega_n) F(\omega_n;\omega_k) \right) \right|^2 , \tag{A2}$$

where $\mathcal{F}^{-1}$ stands for the discrete inverse Fourier transform, i.e. $E^n_{i,j} = \mathcal{F}^{-1}\hat{E}_{i,j}(\omega_n)$. On the other hand, we can obtain the time-averaged near field of such a transverse mode by using a similar filtering technique

$$\overline{P_k}(x_i, y_j) \equiv \frac{1}{N} \sum_n \left| \mathcal{F}^{-1} \left(\hat{E}_{i,j}(\omega_n) F(\omega_n;\omega_k) \right) \right|^2 . \tag{A3}$$

REFERENCES

1. T. Ackemann, S. Barland, M. Cara, S. Balle, J.R. Tredicce, R. Jäger, M. Grabherr, M. Miller and K.J. Ebeling, "Spatial mode structure of bottom-emitting broad-area vertical-cavity surface-emitting lasers", *J. Opt. B: Quantum and Semiclass. Opt.* **2**, pp. 406-412, 2000.
2. K.H. Hahn, M.R. Tan, Y.M. Houng, and S.Y. Wang, "Large area multitransverse mode VCSELs for modal noise reduction in multimode fiber systems", *Electron. Lett.* **29**, pp. 1482, 1993.
3. W. Nakwaski and R.P. Sarzala, "Transverse modes in gain-guided vertical-cavity surface-emitting lasers", *Opt. Comm.* **148**, pp. 63-69, 1998.
4. S. Balle, "Simple analytical approximations for the gain and refractive index spectra in quantum-well lasers", *Phys. Rev. A* **57**, pp. 1304-1312, 1998.
5. J. Martín-Regalado, S. Balle and M. San Miguel, "Polarization and transverse-mode dynamics of gain-guided vertical-cavity surface-emitting lasers", *Opt. Lett.* **22**, pp. 460-462, 1997.
6. W. Nakwaski and M. Osinski, "Thermal properties of vertical-cavity surface-emitting semiconductor lasers", *Progress in Optics* XXXVIII, Ed. E. Wolf, pp. 165-262, 1998.

7. J. Mulet, S. Balle, C.R. Mirasso and M. San Miguel, "Influence of thermal lensing on the transverse mode properties of gain-guided VCSELs", *In preparation.*
8. M. San Miguel, S. Balle, J. Mulet, C.R. Mirasso, E. Tolkachova and J.R. Tredicce, "Combined effects of semiconductor gain dynamics, spin dynamics and thermal shift in polarization selection in VCSELs", *Proc. of SPIE* **3944**, pp. 242-251, 2000.
9. S. Balle, E. Tolkachova, M. San Miguel, J.R. Tredicce, J. Martín-Regalado and A. Gahl, "Mechanisms of polarization switching in single-transverse mode VCSELS: Thermal shift and nonlinear semiconductor dynamics", *Opt. Lett.* **24**, pp. 1121-1123, 1999.
10. O. Buccafusca, J.L.A. Chilla, J.J. Rocca, S. Feld, C. Wilmsen, V. Morozov and R. Leibenguth, "Transverse mode dynamics in vertical-cavity surface emitting lasers excited by fast electrical pulses", *Appl. Phys. Lett.* **68**, pp. 590-592, 1996.
11. O. Buccafusca, J.L.A. Chilla, J.J. Rocca, P. Brusenbach and J. Martín-Regalado, "Transient Response of vertical-cavity surface-emitting lasers of different active-region diameters", *IEEE Journal of Quantum Electron.* **35**, pp. 608-615, 1999.
12. M. Giudici, J.R. Tredicce, G. Vaschenko, J.J. Rocca, and C.S. Menoni, "Spatio-temporal dynamics in vertical cavity surface emitting lasers excited by fast electrical pulses", *Opt. Comm.* **158**, pp. 313-321, 1998.
13. A.W. Snyder and J.D. Love, "Optical waveguide theory", *Ed. Chapman and Hall*, (London), 1983.
14. You can access to some movies at http://www.imedea.uib.es/Photonics/research_topics/trans_pol/index.html
15. J. Mulet, S. Balle, C.R. Mirasso and M. San Miguel, *In preparation.*